Applied Catalysis B: Environmental 324 (2023) 122188

Contents lists available at ScienceDirect

Applied Catalysis B: Environmental

journal homepage: www.elsevier.com/locate/apcatb

Selectively efficient removal of micropollutants by N-doped carbon modified catalytic ceramic membrane: Synergy of membrane confinement and surface reaction

Yufei Zhen [a], Zhiqiang Sun [a,*], Hang Qie [a], Yixuan Zhang [a], Caihong Liu [b], Dongwei Lu [a,*], Wei Wang [a], Yu Tian [a], Jun Ma [a]

[a] State Key Laboratory of Urban Water Resources and Environment, Harbin Institute of Technology, Harbin 150090, People's Republic of China
[b] Key Laboratory of Eco-environments in Three Gorges Reservoir Region, Ministry of Education, School of Urban Construction and Environmental Engineering, Chongqing University, Chongqing 400044, People's Republic of China

ARTICLE INFO

Keywords:
Peroxymonosulfate
N-doped carbon
Membrane
Surface reaction
Confinement

ABSTRACT

Surface-dependent nonradical oxidation of N-doped carbon (NC)-based peroxymonosulfate (PMS) system features high stoichiometric efficiency and target degradation selectivity. However, these are severely limited by the ineffective mass transfer of organics and PMS to NC surface. Herein, we utilize membrane confinement to enhance the interaction between organics/PMS and NC catalyst, and propose the synergy mechanism of surface reaction and membrane confinement towards organics removal. The NC catalyst layer is firstly uniformly loaded throughout the ceramic membrane (NC@CM) via an innovative simultaneous polymerization-coating method. As expected, NC@CM/PMS system significantly expedites the surface reaction dominant oxidation in the filtration-through mode, and its kinetics constant for bisphenol A removal is 3700 times higher than that of NC powder/PMS system. Moreover, it has high selectivity in removal of targeted organics such as BPA (81–100 % removal rate) under various interferences (anions, NOM, water sources) due to the corporation of surface reaction and membrane sieving effect. Mechanism study reveals that the synergy of membrane confinement and surface reaction of NC@CM/PMS system removes large size disturbance and reinforces mass transfer process of reactive species towards target organics, and promotes the generation and transformation of reactive species on the NC surface. Our system can selectively and efficiently remove targeted micropollutants with strong anti-interference capability, which is of great significance in practical application.

1. Introduction

Peroxymonosulfate (PMS) activation is perceived as a potential advanced oxidation process (AOP) for remediation of emerging toxic micropollutants (e.g., bisphenol A) in surface and ground water [1–4]. Various PMS-activation catalysts, as core component in this process, have been explored for promoting electron transfer and reactive species production from PMS precursors [5,6]. Compared to the homogeneous catalysts which employ dissolved transition metals as benchmark in PMS activation, heterogeneous metal catalysts have advantages of simple separation, low cost, and absence of sludge generation [7–9]. Nevertheless, some obstacles still limit their widespread applications: (i) the inevitable leaching of toxic metal ions leads to the secondary pollution risk; (ii) the inferior tunability of the coordination structure of metal atoms hinders the exploitation of catalytic activity [10].

Recently, N-doped carbon (NC), typical heteroatom doped carbonaceous materials, have become emerging heterogenous catalysts to overcome the mentioned drawbacks of traditional metal-based catalysts [11]. The introduction of N dopant can effectively regulate the spin density and charge distribution within the conjugated carbon network, inducing outperformed activity while ensuring safety of the treatment process [12]. Moreover, owing to the unique band structure of sp^2 carbons tailored by electron-rich N dopants, the N-doped carbon catalyst is demonstrated to primarily mediate a surface reaction pathway in PMS activation, where organics are degraded via an electron-transfer pathway over the conducted carbon surface [13,14]. This feature remarkably boosts specific selectivity of the target organics and stoichiometric efficiency of the reaction system, which makes NC a

* Corresponding authors.
E-mail addresses: sunhit@hit.edu.cn (Z. Sun), lvdongwei@hit.edu.cn (D. Lu).

https://doi.org/10.1016/j.apcatb.2022.122188
Received 13 September 2022; Received in revised form 2 November 2022; Accepted 14 November 2022
Available online 16 November 2022

particularly promising catalyst in PMS activation for water treatment [3]. However, the surface reaction dominant AOPs is restricted by mass transfer among PMS, organics and NC in heterogeneous reactive system because the attachment of organics and PMS from bulk aqueous phase onto NC surface is extremely slow [15].

One strategy to enhance mass transfer process of surface dominant reaction is to confine the reactive substances in a spatial space, where the reaction occurs with concentrated reactive substances and short transfer paths [16]. Loading nanocatalysts into the membrane is a simple construction method of confinement reaction system, which has attracted great attentions [17,18]. This catalytic membrane reactor highly accelerates the performance of heterogeneous catalysts in AOPs for selective removal of organic micropollutants [19]. However, the existing preparation methods for NC-based catalytic membrane reactor, such as blending or surface coating of bulk nanocatalysts inevitably cause the destruction of membrane structure, blockage of inner pores and uneven distribution of catalysts, leading to unsatisfactory performance for both permeation and catalytic activity [17,19–21]. Furthermore, although the effect of spatial confinement on radical reaction has been well studied [16,22], the promoting mechanism of spatial confinement has not been clearly studied on surface reaction dominant AOPs of NC-based catalytic membrane reactor, in which spatial condition has greatly influences on the surface reactive species [23].

Based on above analysis, we propose an innovative simultaneous polymerization-coating method to prepare N-doped carbon modified ceramic membrane (NC@CM) with uniform catalyst layer and adequate active sites inside of the membrane. Dopamine is used as a NC precursor, as it can fully infiltrate into membrane pores and gradually polymerize into a uniform coating layer of polydopamine (PDA), thus constructing a well-structured NC-based membrane reactor after being annealed [13]. The catalytic performance and mechanism of NC-based membrane reactor are explored for PMS activation to degrade BPA in a filtration-through mode. Meanwhile, the promoting mechanism of integrating membrane confinement with surface reaction dominant AOPs for micropollutant removal is systematically studied and proposed. Finally, the NC@CM/PMS system is evaluated to selectively and efficiently remove the micropollutants under various interferences, which highlights the critical roles of membrane confinement and surface reaction in practical application.

2. Experimental section

2.1. Materials

Dopamine hydrochloride ($C_8H_{11}NO_2$·HCl, >98 %), Tris-buffer, 5,5-dimethyl-1-pyrroline (DMPO, >99.0 %), 2,2,6,6-tetramethyl-4-piperidinol (TEMP), furfuryl alcohol (FFA), and bisphenol A (BPA) were purchased from Sigma-Aldrich Co. Ltd. Peroxymonosulfate ($2KHSO_5·KHSO_4·K_2SO_4$, PMS), absolute methanol (MeOH, 99.5 %), t-butanol (TBA, 99 %), ammonia solution (NH_4OH, 25 %), potash dichromate ($K_2Cr_2O_7$), and polyethylene oxide (PEO, M_w = 50–500 kDa) were supplied by Aladdin Co. Ltd. The Suwannee River NOM was purchased from the International Humic Substances Society (USA). The substrate ceramic membrane (CM, MWCO = 300 kDa, d = 4.7 cm, thickness = 25 mm) made of TiO_2 and ZrO_2 was obtained from TAMI. Deionized (DI) water was supplied by a Milli-Q purification system (Millipore, Billerica, MA). All the above chemicals were used without further purification.

2.2. Synthesis of NC@CM

The NC@CM was synthesized by a mild simultaneous polymerization-coating process (Fig. 1a). Specifically, a dopamine solution (2 g L^{-1}) under Tris-buffering (10 mM) at pH of 8 was mixed with alcohol at the ratio of 5:1. Then, the substrate membrane was hanged and dipped into the solution for fixed time (6, 12 and 24 h) at ambient temperature to obtain PDA@CM. Finally, the NC@CM was synthesized after annealing of PDA@CM in tube furnace at 800 °C for 1 h with a

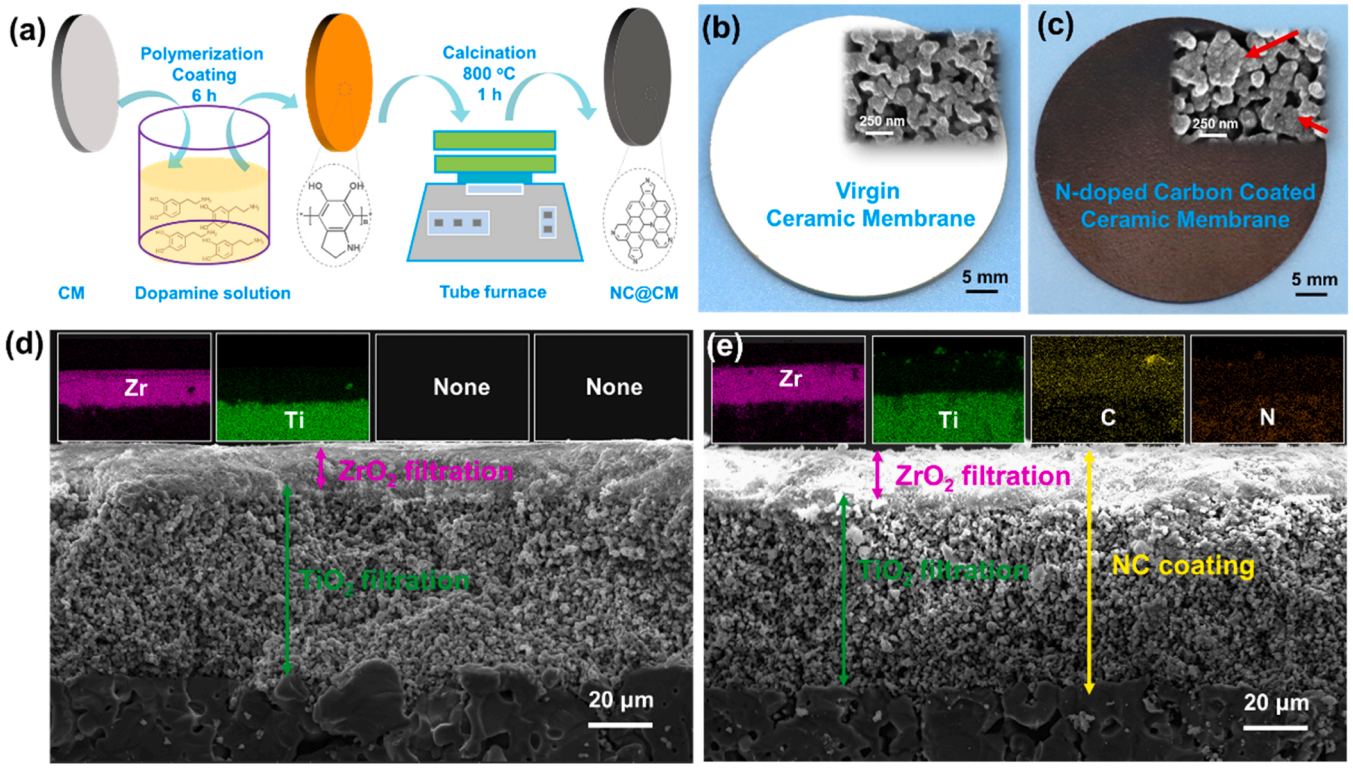

Fig. 1. (a) Schematic diagram of NC@CM fabrication; The digital photos and SEM images of (b) CM and (c) NC@CM; The SEM and EDS-mapping images of (d) CM and (e) NC@CM.

heating rate of 5 °C min^{-1} in Ar atmosphere. The NC@CM is named according to the style of NC@CM (xh) where x represents the polymerization time in dopamine solution. Unless specified, the NC@CM refers to NC@CM (6 h) in the following statement. As control, the NC powder was also prepared (Fig. S2) and the procedure is shown in Text S1.

2.3. Characterizations

The membrane morphology was observed by a scanning elector microscope (SEM, FEI, Quanta 200 F, USA). The Fourier Transform Infrared Spectrometer (FTIR, Perkin-Elmer, USA), X-ray diffraction patterns (XRD, X'Pert Pro, PANalytical, Holland), Raman spectra (Nanofinder 30 R, Tokyo), BET (Micromeritics, ASAP 2020, USA) and X-ray photoelectron spectroscopy (XPS, ULVCA-PHI, PHI-5700, USA) were employed to detect the physic-chemical information of prepared membranes. The pore size of prepared membrane was determined by mercury intrusion method using mercury injection apparatus (Micromeritics, Auto Pore V, USA). For obtaining the loading dosage of NC on NC@CM, the thermogravimetric analysis (TGA, Metler Toledo, SDTA851E, Switzerland) was conducted at 800 °C with a heating rate of 5 °C min^{-1} under air atmosphere.The specific operation parameters are shown in Text S2.

2.4. Membrane performance tests

The filtration-through mode tests were conducted in a dead-end filtration system as shown in Fig. S1. In a typical membrane catalytic experiment, the feed solution containing PMS (0.01 g L^{-1}), BPA (2 mg L^{-1}), phosphate buffer (pH = 7, 5 mM) and other contaminants (e.g., quenching agents, NOM, anions etc.) was filtrated through the membrane under different transmembrane pressure (0.05–0.2 MPa) regulated by the height of liquid level. Then, at specific permeate volume intervals, water samples were taken out from effluent using a syringe, filtered through a 0.22 μm polytetrafluoroethylene (PTFE) filter and quenched with 1 M MeOH. The permeate flux through membrane was measured by the digital balance and recorded by the computer immediately. For contrast, the heterogenous catalytic experiment was also conducted in a batch mode with addition of NC powder (2.8 g L^{-1}) under the same reaction condition for 1 h.

The BPA concentration was determined using high-performance liquid chromatography (HPLC, Waters 2695) with a C18 column at λ_{DAD} = 226 nm. The mobile phase was a mixture of MeOH/Milli-Q water (70/30 v/v). The removal of NOM was monitored by TOC analyzer (Analytik Jena Multi N/C 3100, Germany). The reactive species were detected by electron paramagnetic resonance spectrometer (EPR, EMX-8/2.7, Germany, center field: 3480.00 G, sweep width: 100.00 G, static field: 3480.00 G, frequency: 9.751 GHz, power: 4 mW). The interfacial reaction process of PMS on the surface of catalyst was clarified by in-situ Raman spectra (HORIBA, Japan) equipped with a CCD detector using a laser source at excitation wavelength of 532 nm.

3. Results and discussion

3.1. Characterizations

Seen from Fig. 1b and c, the color of the NC@CM changes from white to brownish black after NC is loaded. The NC layer is smooth and compact (pointed by the red arrow), and no obvious difference is observed in the structural characteristic between CM and NC@CM, indicating the even and thin NC coating throughout the surface of CM. Meanwhile, according to the EDS-mapping (Fig. 1d and e), the N and C elements are evenly scattered on the membrane cross-section of NC@CM, again suggesting the uniform distribution of NC within the membrane pore structure. The above results show that the mild simultaneous polymerization-coating method facilitates to form homogenous functional layer on membrane. Because the molecular dopamine can fully infiltrate into the pores of the membrane and effectively avoid the agglomeration and pore blocking phenomenon, in comparison with those bulk carbon materials such as carbon nanotube, graphene, activated carbon, etc. [11,24,25]. This synthesis method significantly expands the surface area and the limited inner space of CM, as the specific surface area of NC@CM (6 h) reaches to 33.81 m^2 g^{-1} (Fig. S3). Moreover, due to the high versatile adhesive capacity of dopamine [26], combing with simultaneous polymerization-coating process, the carbon coating layer formed after calcination is extremely stable on NC@CM, even when suffering from strong ultrasound, acid and base conditions (Fig. S4). Above excellent properties of NC@CM ensure adequate exposure of active sites and durable stability during catalytic oxidation of pollutants.

The XRD patterns of NC@CM (Fig. 2a) show that the characteristic diffraction peaks at ~25° and ~44° assigning to (002) and (100) reflections of hexagonal graphitic structure of carbon are coexisted with the standard diffraction peaks of TiO_2 (PDF# 89-4202) and ZrO_2 (PDF# 49-1642) [20,27]. This result displays that the amorphous carbon along with some crystal graphitic structures is formed after calcination of PDA under high temperature (800 °C) and is coated on the CM substrate [28]. The Raman spectra (Fig. 2b) further confirms the high graphitization of carbon coating layer on NC@CM as evidenced by the low ratio value of D band (defect structure) to G band (graphitic structure) (I_D/I_G=1.04). This is benefited from that the C atoms in PDA which mainly locate in the ring can form sp^2 C more easily than those outside the ring during the calcination [29]. These favorable features of carbon coating layer will contribute to the high catalytic performance of NC@CM [27]. The actual loading dosage of carbon in NC@CM (6 h) was also quantified by TGA (Fig. 2c), and the weight is 3.7 wt% of that of NC@CM (15.45 ± 0.23 g). Specially, with a carbon loading of ~0.57 g in an inner volume of 4.20e-5 L (Text S3), the concentration of available catalyst in the confined space of NC@CM is estimated to be 1.35e4 g L^{-1}. This is a very high value, which can accelerate the mass diffusion within NC@CM to a great extent and thus enhance the effectivity of micropollutant removal in AOPs [22].

Further compositional information of the carbon coating layer on NC@CM was obtained from FTIR spectra and XPS analysis. Fig. 2d displays that the peaks at 1498 and 1600 cm^{-1} attributing to the stretching and bending vibration of N-H in the precursor of PDA@CM severely decrease or disappear after calcination. A new stretching vibration band of C-N at 1571 cm^{-1} emerges in NC@CM [30]. This change indicates that the N atoms of N-H groups in PDA have been in situ intercalated into the carbon skeleton and the NC coating layer is successfully formed on NC@CM. Moreover, highly reduction of oxygen-containing groups (C═O 1290 cm^{-1}, C-OH 1066 cm^{-1} and -OH 3200–3500 cm^{-1}) to oxygen-free carbon skeleton (C-H, 1114 cm^{-1}) is observed after calcination of PDA@CM [30], which facilitates formation of graphitic structure of NC coating layer on NC@CM, in consistence with Raman result (Fig. 2b) [31]. These N-doped sites and graphic structures in the carbon skeleton have been proposed as the dominant active centers, leading to the outstanding catalytic performance of PDA-based NC compared to other N-based carbon catalysts [13]. The chemical composition of NC@CM is shown in Fig. 2e, C 1s (284.8 eV) and N 1s (400.6 eV) peaks are clearly presented in comparison with that of CM. Additionally, the atomic ratio of N to C is as high as 9.5 %, which is a relative higher content than that of those NCs reported in current researches [32,33]. This is derived from the superior chemical property of dopamine and the special preparation process of NC@CM, as discussed in our previous study [27]. The N atoms (Fig. 2f) in carbon skeleton are also sp^2-hybridized and composed of pyridinic N (6.9 %, 398.2 eV), pyrrolic N (13.8 %, 399.6 eV), graphitic N (72.3 %, 400.9 eV) and nitric oxides (7.0 %, 402.0 eV). High content of electron rich graphitic N in carbon structure is known to serve as "electron-mobility" region for regulating the penetration and transfer of electrons, thus playing an important role in catalytic activity of the NC@CM in PMS

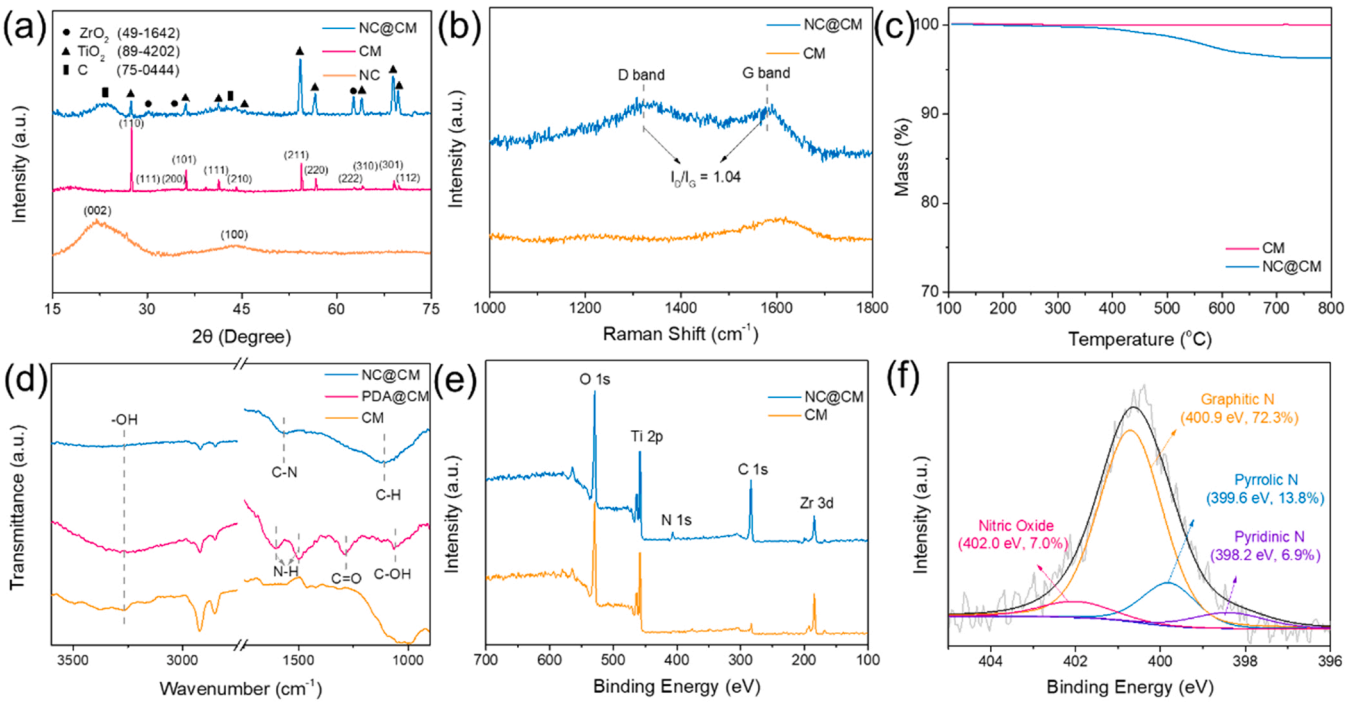

Fig. 2. (a) XRD patterns, (b) Raman spectra, (c) TGA curves, (d) FTIR spectra and (e) XPS survey of prepared membranes; (f) deconvoluted N 1s spectra of NC@CM.

activation [13,27]. These above preferable properties provide more guarantees for micropollutant removal in the NC@CM/PMS system.

3.2. Performances

The catalytic performance of NC@CM was evaluated by filtering a synthetic feed solution containing PMS and BPA at pH 7.0 through the membrane samples. Using as-prepared NC@CMs with PDA loading time from 0 to 24 h (Fig. 3a), it is observed that the permeate flux decreases gradually with increasing loading time, but the complete removal of BPA can be achieved when loading time is over 6 h. This result suggests that 6 h is enough for full coverage of NC on pore surface of NC@CM. In this case, the complete removal of BPA only requires retention time as low as about 21.0 s (Fig. S5a). NC@CM/PMS system outperforms most of the reported carbon-based heterogenous PMS activation systems, and is even better than some metal oxides-modified CM/PMS systems [21, 34]. Three possible reasons may count for this excellent performance: (I) the catalysts layer is uniform and complete within NC@CM derived from the simultaneous polymerization-coating method in this study, as identified in Figs. 1 and 2; (II) the nanoconfinement effect within NC@CM induces effective reactions among BPA, PMS and NC catalysts [16]; (III) the synergistic effect between surface reaction mechanism and membrane confinement nature endows NC@CM/PMS system with selectively efficient removing ability of micropollutants.

The PMS-activation performance of NC@CM was compared with that of pristine CM (a filtration-through PMS-activation mode), NC powder and bulk NC@CM (a batch heterogenous PMS-activation mode). The BPA concentration as a function of retention/reaction time is shown in Fig. 3b. BPA removal by pristine substrate CM alone is much less than that by NC@CM under filtration-through mode, verifying the superb activity of NC coating layer in PMS activation. Note that when treating the same volume (200 mL) of water sample, the filtration-through PMS-activation mode for NC@CM has obviously higher efficiency in shorter reaction time (Figs. S5a and S5b) than that of batch PMS-activation mode for NC powder and NC@CM. The first-order rate constant (k_{obs}, Text S4, Fig. S5c) of BPA removal by NC@CM in filtration-trough mode is 0.29 s^{-1}, about 3700 and 6700 times higher than that by NC powder and NC@CM in batch mode, respectively. Such a prominent performance is attributed to the nanoconfinement effect within NC@CM in the filtration-though mode thus enhancing the kinetics of BPA removal [16].

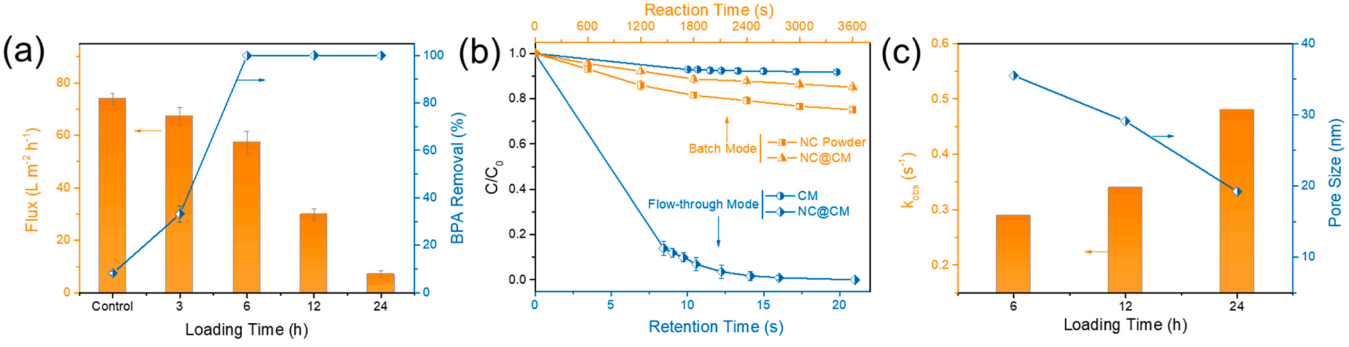

Fig. 3. (a) The water flux and the removal of BPA versus PDA loading time in NC@CM/PMS system; (b) the BPA degradation versus reaction time under different systems; (c) the first-order reaction constant rate of BPA degradation and pore size versus PDA loading time in NC@CM/PMS system. Conditions (a) pressure = 0.05 MPa, $[PMS]_0$ = 0.01 g L^{-1}, $[BPA]_0$ = 2 mg L^{-1}, permeate volume = 200 mL, pH = 7; (b) pressure = 0.05–0.20 MPa, NC powder = 2.8 g L^{-1}, reaction volume = 200 mL.

The activation of PMS by carbonaceous materials (e.g., NC) for organic pollutant removal is tightly related to the interaction of organics and PMS on catalyst surface [35]. In the filtration-through mode, the thermal motion of BPA and PMS is confined in a nanoscale membrane pores, so that the diffusion distance of these molecules in nano-sized inter spacings should be significantly decreased. The steep concentration gradient (perpendicular to the flow direction) propels both BPA and PMS molecules from the center to the boundaries, causing the higher concentration of BPA and PMS around pore surface of NC@CM (Fig. S5d) [36]. This process enhances the effective collision of organics and PMS onto NC coating layer, and promotes the following BPA degradation [16,22].

To confirm the critical role of nanoconfinement effect in catalytic performance of NC@CM, the kinetics of BPA removal in NC@CM (12 h)/PMS and NC@CM (24 h) /PMS were also evaluated. As shown in Fig. 3c, the pore sizes of NC@CMs gradually decrease from ~35.5 to ~19.2 nm (Fig. S6, Table S1) with the PDA loading time increasing from 6 to 24 h. As expected, the k_{obs} values show an obvious negative relationship with pore sizes, verifying that the BPA removal kinetics increases with the enhancement of the nanoconfinement effect within NC@CM. Though the specific surface area of NC@CM (24 h) (12.55 m^2 g^{-1}, Fig. S5e) is lower than that of NC@CM (6 h), the k_{obs} value (Figs. 3c and S5f) of NC@CM (24 h) displays much higher than that of NC@CM (12 h) and NC@CM (6 h) (i.e., 0.48 s^{-1} VS. 0.34 s^{-1} VS. 0.29 s^{-1}). This result again confirms the critical role of nanoconfinement effect on catalytic performance of NC@CM [16].

3.3. Mechanism

Two kinds of pathways namely radical (•OH, $SO_4^{\bullet-}$) and nonradical ($^1O_2$, PMS-catalyst complex, surface persistent free radical) oxidation would occur in carbon-based PMS AOPs [12,13,23,37,38]. Typical radical scavenging agents of tert-butyl alcohol (TBA, $k_{\bullet OH} = 5.2 \times 10^{10}$ M^{-1} s^{-1}) and methanol (MeOH, $k_{\bullet OH} = 9.7 \times 10^8$ M^{-1} s^{-1}, $k_{SO_4^{\bullet-}} = 2.5 \times 10^7$ M^{-1} s^{-1}) were added into the NC@CM/PMS/BPA reaction solution to scavenge •OH and both •OH/$SO_4^{\bullet-}$, respectively [19]. As shown in Fig. 4a, either TBA or MeOH shows negligible influence (~10 % inhabitation) on BPA degradation, indicating that the steady state concentrations of •OH and $SO_4^{\bullet-}$ are extremely low in NC@CM/PMS system. This result is consistent with that of EPR measurement (Fig. 4b), as no DMPO-•OH and DMPO-$SO_4^{\bullet-}$ adducts can be observed. However, another characteristic signal of DMPOX with an intensity ratio of 1:2:1:2:1:2:1 is observed. Due to the lack of •OH and $SO_4^{\bullet-}$, DMPOX is considered to be produced via the direct oxidation of DMPO by nonradical reactive species [39].

As EPR results with the addition of TEMP show (Fig. 4b), the typical three-line signal with equal intensities of TEMP-$^1O_2$ is detected, indicating the presence of $^1O_2$. But there is only little inhibitation (~20 %) of BPA degradation (Fig. 4a) when quenching $^1O_2$ with FFA, suggesting that $^1O_2$ is not the dominant nonradical reactive species in NC@CM/PMS system. Ren et al. [12] has proposed that in carbon-based PMS AOPs, especially with NC, PMS-catalyst complex can serve as reactive species to induce single electron transfer nonradical oxidation process for pollutant degradation. In the PMS-catalyst complex mechanism, the activated PMS is supposed to attach onto the surface of catalyst to form complexes, and PMS can not decompose without pollutant in the reaction system. While the obvious decomposition of PMS is observed in pure NC@CM/PMS system without addition of BPA (Fig. S5d). Therefore, other nonradical reactive species rather than $^1O_2$ and PMS-catalyst complex dominate the BPA degradation in NC@CM/PMS system.

We recently identified the surface persistent free radicals (PFRs) as crucial intermediates of nonradical process in NC/PMS system [13]. To further verify whether PFRs are formed in NC@CM/PMS system, potassium dichromate ($K_2Cr_2O_7$) was used as a scavenger for PFRs [40,41]. Notably, the BPA degradation is almost completely inhibited in presence of $K_2Cr_2O_7$ (Fig. 4a), suggesting PFRs are majorly responsible for the pollutant oxidation in NC@CM/PMS system. In addition, when using the NC powder scraped from NC@CM as catalyst to react with PMS, an obvious single-resonance signal can be detected in EPR measurement with g value of 2.0037 (Fig. 4b), yet absent once adding $K_2Cr_2O_7$. This result further confirms PFRs to be the dominant reactive species for BPA degradation [13,41].

The in-situ Raman was employed to investigate the reaction among PMS, NC@CM and BPA. As shown in Fig. 4c, for pure PMS solution, three peaks at 887, 1058, and 980 cm^{-1} are observed, representing the characters of HSO_5^- and SO_4^{2-} [42]. In addition, two weak peaks at 808 and 838 cm^{-1} are found, which are attributed to the peroxy-species (i.e., H_2O_2 and $^1O_2$) and free radicals (i.e., •OH and $SO_4^{\bullet-}$). When PMS reacts with NC@CM, two peaks at 808 and 838 cm^{-1} disappear, consistent with the EPR result. This is probably because •OH and $SO_4^{\bullet-}$ attack on NC surface and transform into PFRs [13]. In our previous work, the •OH and $SO_4^{\bullet-}$ can be detected in the NC/PMS system, yet not detected in NC@CM/PMS system (filtration-through mode). It can be deduced that the nanoconfinement effect in NC@CM mainly accounts for this difference, because the generated •OH and $SO_4^{\bullet-}$ in membrane pores are confined in the nanoscale domains, avoiding diffusion into the bulk solution [36]. This case accelerates the quick transformation of •OH and $SO_4^{\bullet-}$ into PFRs and causes the extreme low steady-state concentration of •OH and $SO_4^{\bullet-}$ in solution. Moreover, the carbon structure of NC@CM changes obviously as I_D/I_G increases from 0.95 to 1.02 when adding BPA. This phenomenon confirms the surface reaction mechanism in NC@CM/PMS system that BPA tends to react with PFRs and further leads to the changes of carbon structure of NC@CM. Overall, membrane confinement not only enhances surface reaction efficiency among the PMS, catalyst and BPA, but also accelerates the generation and transformation of reactive species on the NC surface.

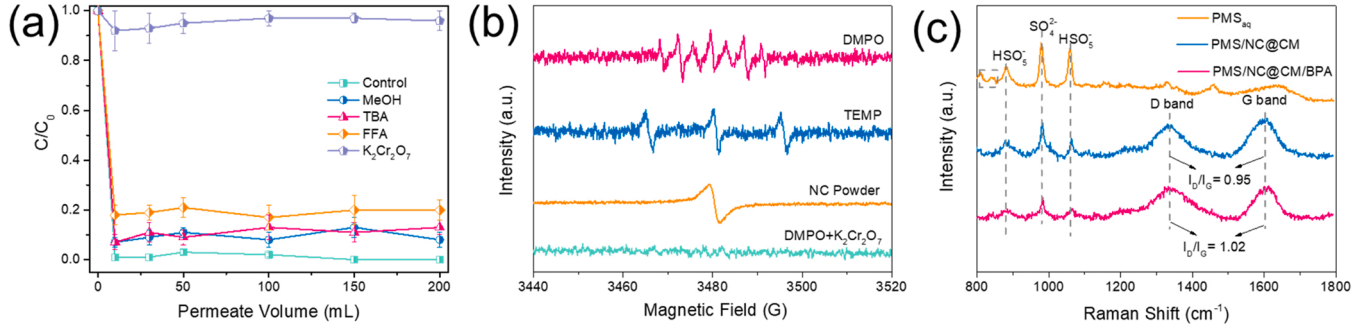

Fig. 4. (a) Quenching effects of different scavengers on BPA degradation in NC@CM/PMS system; (b) EPR signals of PMS activation under different conditions; (c) in-situ Raman spectra of NC@CM/PMS reactive system. Conditions (a) pressure = 0.05 MPa, $[PMS]_0 = 0.01$ g L^{-1}, $[BPA]_0 = 2$ mg L^{-1}, $[MeOH]_0 = 0.1$ g L^{-1}, $[TBA]_0 = 0.1$ g L^{-1}, $[FFA]_0 = 0.1$ g L^{-1}, $[K_2Cr_2O_7]_0 = 0.1$ g L^{-1}, permeate volume = 200 mL, pH = 7; (b) $[MeOH]_0 = 0.1$ mM, $[TEMP]_0 = 0.1$ mM, $[K_2Cr_2O_7]_0 = 0.1$ g L^{-1}.

3.4. Applications

The above results show that NC@CM/PMS exhibits attractive performance for BPA degradation. However, in practical applications, the background water usually contains micropollutants with some interfering substances, such as inorganic anions, NOM. As reported, the concomitant anions in water tend to compete with target pollutants to consume reactive species produced in the catalytic process, causing a compromised degradation performance [24]. Conversely, the presence of Cl^-, NO_3^- and HCO_3^- all show negligible influences on BPA degradation in NC@CM/PMS system (Fig. 5a). The traditional AOPs suffer from abominable effect mainly due to the useless consumption of radicals (•OH and $SO_4^{\bullet-}$) by anions in the bulk solution. For NC@CM/PMS, the generated reactive species, PFRs, are confined on the catalyst surface [13], leaving them little chance to interact with anions. Moreover, the NC@CM surface hardly adsorbs hydrophilic substances due to the hydrophobic nature of N dopant [28]. Therefore, the anions are difficult to consume PFRs generated on NC@CM. This is a distinctive advantage of NC@CM/PMS system in comparison with other AOPs.

The exposure of aromatic NOM in AOPs can cause substantial decrease of efficiency for target pollutant degradation, due to the severe quenching ability for reactive species (second order constant for •OH, $10^9 - 10^{10}$ M^{-1} s^{-1}) [20]. Though the reactive rate constant of PFRs with NOM is unknown, it can be observed that more than 80 % BPA degradation is inhibited with addition of 10 mg L^{-1} NOM in batch experiment of NC/PMS (Fig. S7). Fortunately, this negative effect can be largely avoided in NC@CM/PMS system (Fig. 5b), in which the majority of NOM (~77 % TOC, Fig. 5c) can be rejected by the size exclusion with membrane. In such case, generated PFRs inside the pore surface of NC@CM will not be interacted with too much NOM, which in turn facilitates the selective degradation of BPA. It is worth noticing that not only ~81 % BPA degradation is realized, but also ~88 % TOC removal is achieved as well (Fig. 5b and c) in NC@CM/PMS system. The above results indicate that the NC@CM/PMS shows good selectivity for BPA degradation under various interference conditions.

For a sustainable operation with high performance, it is essential to explore the stability of catalytic activity for NC@CM after multiple runs. As shown in Fig. 5d, the activity of NC@CM can be effectively recovered by simple backwashing with DI water for 30 min under 0.02 MPa, presenting only about 10 % loss after five cycles. Such deactivation of NC@CM is believed to be caused by some intermediate products adsorbing or bonding with the active site of catalyst. Reannealing at high temperature is found to be effective to recover the activity of NC@CM, as evidenced by 100 % BPA degradation by NC@CM/PMS after regeneration. This is a special advantage for carbon modified catalytic CM in applications.

The practical application of NC@CM/PMS system for BPA degradation was also evaluated with Songhua River water after filtrating

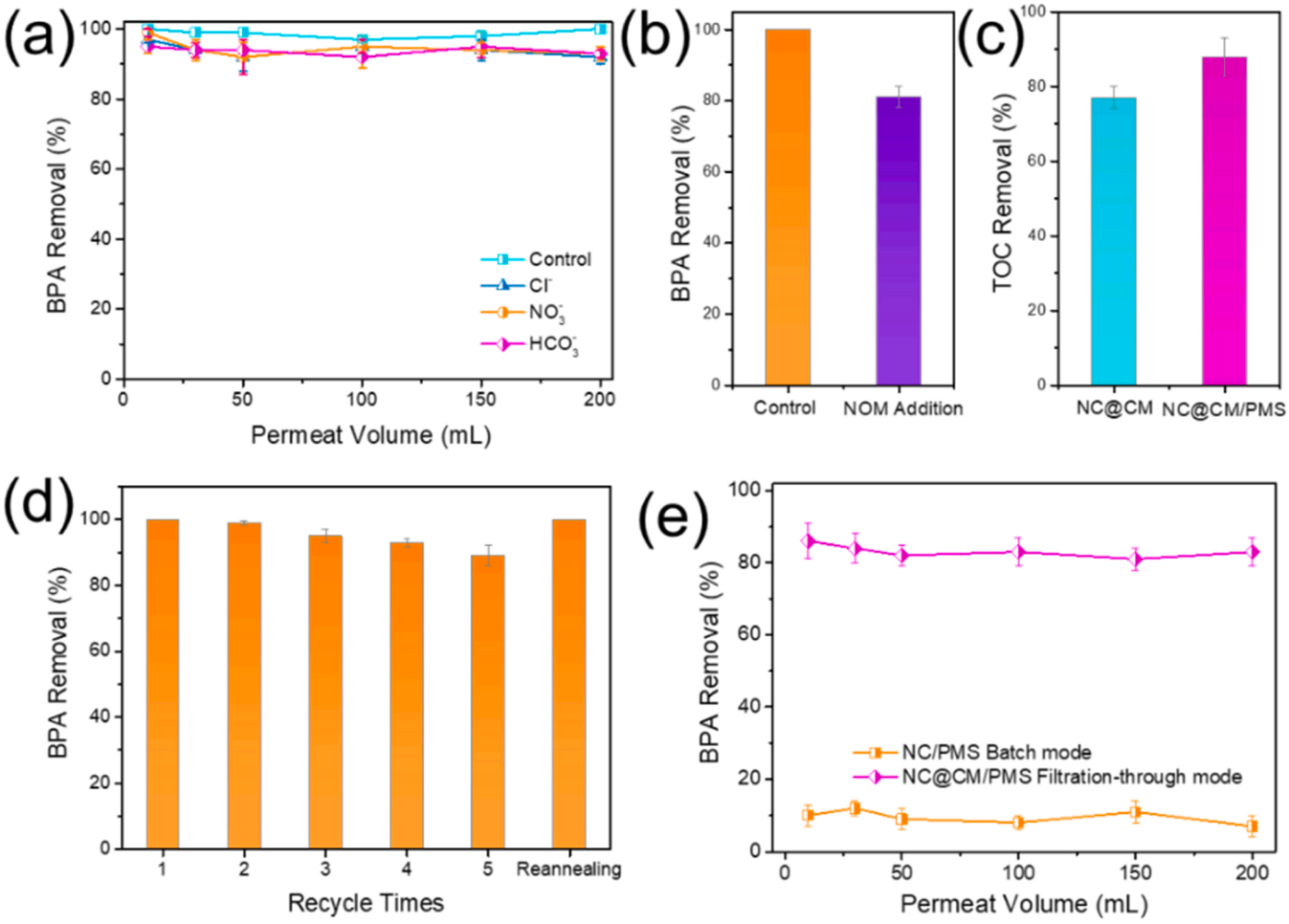

Fig. 5. (a) The effects of different anions on BPA degradation in NC@CM/PMS system; (b) the effect of NOM on BPA degradation in NC@CM/PMS system; (c) the TOC removal for mixture of BPA and NOM in NC@CM and NC@CM/PMS systems; (d) the BPA degradation in NC@CM/PMS system after multiple runs within tap water; (e) the effects of water sources on BPA degradation in NC@CM/PMS system. Conditions (a) pressure = 0.05 MPa, $[PMS]_0$ = 0.01 g L^{-1}, $[BPA]_0$ = 2 mg L^{-1}, $[MeOH]_0$ = 0.1 g L^{-1}, $[anion]_0$ = 10 mM, permeate volume = 200 mL, pH = 7; (b) $[NOM]_0$ = 10 mg L^{-1}; (d) reannealing temperature = 800 °C; (e) no pH buffering in river water.

through quartz sand filter (detailed properties in Table S2). As shown in Fig. 5e, a well satisfactory BPA degradation efficiency is obtained (~83 %) in NC@CM/PMS system, whereas, nearly complete loss of BPA degradation is observed with NC/PMS in the batch mode. This result again confirms the above conclusion that the NC@CM/PMS system possesses not only high capacity for BPA degradation but also superb anti-interference characteristic. Overall, the combined effect of surface reaction and membrane confinement of NC@CM/PMS system demonstrates a great potential in the selectively efficient removal of micropollutants in practical applications.

4. Conclusions

This study systematically investigates the availability of integrating surface dominant AOPs with membrane reactor for selectively efficient degradation of micropollutants. Firstly, an innovative simultaneous polymerization-coating method is employed for preparation of the N-doped carbon modified ceramic membrane (NC@CM). Characterization studies show that a uniform NC catalyst layer is loaded throughout the membrane. This feature guarantees adequate exposure of active sites in the limited inner space of CM during AOPs, thus inducing superb activity for PMS activation on BPA degradation. Secondly, mechanism study reveals that the surface persistent free radicals (PFRs) dominate the organic micropollutant oxidation in NC@CM/PMS system, and their generation are highly accelerated by the nanoconfinement effect within membrane pore. Driven by such particular surface reaction process, the advantage of membrane confinement in membrane reactor is much more highlighted, because the PFRs formation and the subsequent AOPs are more dependent on the mass transfer efficiency than other radical dominant AOPs. Finally, the practical application experiments show that the NC@CM/PMS system has strong anti-interference capability under various conditions and good stability for reuse in recycle tests. Comprehensively, the synergy between surface reaction dominant oxidation and membrane confinement plays the critical role in selectively efficient removal of micropollutants in NC@CM/PMS system. This study provides a potential application direction of surface reaction dominant AOPs in aqueous environment.

CRediT authorship contribution statement

Yufei Zhen: Conceptualization, Data curation, Formal analysis, Writing – original draft. **Zhiqiang Sun:** Writing – review & editing, Conceptualization. **Hang Qie** : Visualization, Investigation. **Yixuan Zhang:** Data curation, Software, Visualization. **Caihong Liu:** Investigation. **Dongwei Lu:** Software, Visualization. **Wei Wang:** Project administration. **Yu Tian:** Project administration. **Jun Ma:** Supervision.

Declaration of Competing Interest

The authors declare that they have no known competing financial interests or personal relationships that could have appeared to influence the work reported in this paper.

Data availability

Data will be made available on request.

Acknowledgement

This work was financially supported by the National Natural Science Foundation of China (Grant No. 52000050 and 51908162), Science Foundation of Heilongjiang Province (Grant No. LH2020E053), Postdoctoral Science Foundation of China (Grant No. 2020M670913), Heilongjiang Postdoctoral Fund (Grant No. LBH-Z20063) and State Key Laboratory of Urban Water Resource and Environment (Harbin Institute of Technology) (Grant No. 2021TS22).

Appendix A. Supporting information

Supplementary data associated with this article can be found in the online version at doi:10.1016/j.apcatb.2022.122188.

References

[1] W. Wang, H. Wang, G. Li, T. An, H. Zhao, P.K. Wong, Catalyst-free activation of persulfate by visible light for water disinfection: efficiency and mechanisms, Water Res. 157 (2019) 106–118.
[2] S. Zhu, X. Li, J. Kang, X. Duan, S. Wang, Persulfate activation on crystallographic manganese oxides: mechanism of singlet oxygen evolution for nonradical selective degradation of aqueous contaminants, Environ. Sci. Technol. 53 (2019) 307–315.
[3] J. Lee, U. von Gunten, J.H. Kim, Persulfate-based advanced oxidation: critical assessment of opportunities and roadblocks, Environ. Sci. Technol. 54 (2020) 3064–3081.
[4] W. Wang, H. Wang, G. Li, P.K. Wong, T. An, Visible light activation of persulfate by magnetic hydrochar for bacterial inactivation: efficiency, recyclability and mechanisms, Water Res. 176 (2020), 115746.
[5] W. Liu, C. Nie, W. Li, Z. Ao, S. Wang, T. An, Oily sludge derived carbons as peroxymonosulfate activators for removing aqueous organic pollutants: performances and the key role of carbonyl groups in electron-transfer mechanism, J. Hazard. Mater. 414 (2021), 125552.
[6] D. Xia, R. Yin, J. Sun, T. An, G. Li, W. Wang, H. Zhao, P.K. Wong, Natural magnetic pyrrhotite as a high-efficient persulfate activator for micropollutants degradation: radicals identification and toxicity evaluation, J. Hazard. Mater. 340 (2017) 435–444.
[7] C. Wang, J. Kim, V. Malgras, J. Na, J. Lin, J. You, M. Zhang, J. Li, Y. Yamauchi, Metal-organic frameworks and their derived materials: emerging catalysts for a sulfate radicals-based advanced oxidation process in water purification, Small 15 (2019), e1900744.
[8] G. Wen, D. Zhao, X. Xu, Z. Chen, T. Huang, J. Ma, Inactivation of fungi from four typical genera in groundwater using PMS/Cl^- system: efficacy, kinetics and mechanisms, Chem. Eng. J. 357 (2019) 567–578.
[9] L. Ling, Z. Li, J. Fang, C. Shang, Controlling bromate formation in the Co(II)/peroxymonosulfate process by ammonia, chlorine-ammonia and ammonia-chlorine pretreatment strategies, Water Res. 139 (2018) 220–227.
[10] C. Chu, J. Yang, X. Zhou, D. Huang, H. Qi, S. Weon, J. Li, M. Elimelech, A. Wang, J. H. Kim, Cobalt single atoms on tetrapyridomacrocyclic support for efficient peroxymonosulfate activation, Environ. Sci. Technol. 55 (2021) 1242–1250.
[11] M. Pedrosa, G. Drazic, P.B. Tavares, J.L. Figueiredo, A.M.T. Silva, Metal-free graphene-based catalytic membrane for degradation of organic contaminants by persulfate activation, Chem. Eng. J. 369 (2019) 223–232.
[12] W. Ren, G. Nie, P. Zhou, H. Zhang, X. Duan, S. Wang, The intrinsic nature of persulfate activation and N-doping in carbocatalysis, Environ. Sci. Technol. 54 (2020) 6438–6447.
[13] Y. Zhen, S. Zhu, Z. Sun, Y. Tian, Z. Li, C. Yang, J. Ma, Identifying the persistent free radicals (PFRs) formed as crucial metastable intermediates during peroxymonosulfate (PMS) activation by N-doped carbonaceous materials, Environ. Sci. Technol. 55 (2021) 9293–9304.
[14] P. Hu, H. Su, Z. Chen, C. Yu, Q. Li, B. Zhou, P.J.J. Alvarez, M. Long, Selective degradation of organic pollutants using an efficient metal-free catalyst derived from carbonized polypyrrole via peroxymonosulfate activation, Environ. Sci. Technol. 51 (2017) 11288–11296.
[15] M. Carballa, G. Fink, F. Omil, J.M. Lema, T. Ternes, Determination of the solid-water distribution coefficient (Kd) for pharmaceuticals, estrogens and musk fragrances in digested sludge, Water Res. 42 (2008) 287–295.
[16] S. Zhang, M. Sun, T. Hedtke, A. Deshmukh, X. Zhou, S. Weon, M. Elimelech, J. H. Kim, Mechanism of heterogeneous Fenton reaction kinetics enhancement under nanoscale spatial confinement, Environ. Sci. Technol. 54 (2020) 10868–10875.
[17] Y. Wang, Y. Zhang, J. Wang, Nano spinel $CoFe_2O_4$ deposited diatomite catalytic separation membrane for efficiently cleaning wastewater, J. Membr. Sci. 615 (2020), 118559.
[18] Q. Zhao, D. Lu, H. Jiang, Y. Zhao, Y. Sun, Z. Li, M. Yang, P. Wang, J. Ma, Peroxymonosulfate-based cleaning technology for metal oxide-coated ceramic ultrafiltration membrane polluted by Alcian Blue 8GX dye: radical and non-radical oxidation cleaning mechanism, J. Membr. Sci. 573 (2019) 210–217.
[19] J. Xie, Z. Liao, M. Zhang, L. Ni, J. Qi, C. Wang, X. Sun, L. Wang, S. Wang, J. Li, Sequential ultrafiltration-catalysis membrane for excellent removal of multiple pollutants in water, Environ. Sci. Technol. 55 (2021) 2652–2661.
[20] Y. Zhao, D. Lu, C. Xu, J. Zhong, M. Chen, S. Xu, Y. Cao, Q. Zhao, M. Yang, J. Ma, Synergistic oxidation - filtration process analysis of catalytic $CuFe_2O_4$-tailored ceramic membrane filtration via peroxymonosulfate activation for humic acid treatment, Water Res. 171 (2020), 115387.
[21] H. Wu, X. Xu, L. Shi, Y. Yin, L.C. Zhang, Z. Wu, X. Duan, S. Wang, H. Sun, Manganese oxide integrated catalytic ceramic membrane for degradation of organic pollutants using sulfate radicals, Water Res. 167 (2019), 115110.
[22] S. Zhang, T. Hedtke, Q. Zhu, M. Sun, S. Weon, Y. Zhao, E. Stavitski, M. Elimelech, J. H. Kim, Membrane-confined iron oxychloride nanocatalysts for highly efficient heterogeneous Fenton water treatment, Environ. Sci. Technol. 55 (2021) 9266–9275.
[23] S. Zhu, X. Huang, F. Ma, L. Wang, X. Duan, S. Wang, Catalytic removal of aqueous contaminants on N-doped graphitic biochars: inherent roles of adsorption and nonradical mechanisms, Environ. Sci. Technol. 52 (2018) 8649–8658.

[24] Z. Song, J. Sun, W. Wang, Z. Wang, Y. Zhang, B. Xu, F. Qi, Stable synergistic decontamination and self-cleaning performance of powerful N-rGO catalytic ozonation membrane: clustering effect of free electrons and role of interface properties, Appl. Catal. B Environ. 283 (2021), 119662.
[25] M. Zhang, C. Xiao, C. Zhang, J. Qi, C. Wang, X. Sun, L. Wang, Q. Xu, J. Li, Large-scale synthesis of biomass@MOF-derived porous carbon/cobalt nanofiber for environmental remediation by advanced oxidation processes, ACS EST Eng. 1 (2021) 249–260.
[26] H. Lee, S.M. Dellatore, W.M. Miller, P.B. Messersmith, Mussel-inspired surface chemistry for multifunctional coatings, Science 318 (2007) 426–430.
[27] Z. Sun, L. Zhao, C. Liu, Y. Zhen, J. Ma, Catalytic ozonation of ketoprofen with in situ N-doped carbon: a novel synergetic mechanism of hydroxyl radical oxidation and an intra-electron-transfer nonradical reaction, Environ. Sci. Technol. 53 (2019) 10342–10351.
[28] Z. Sun, L. Zhao, C. Liu, Y. Zhen, J. Ma, Fast adsorption of BPA with high capacity based on π-π electron donor-acceptor and hydrophobicity mechanism using an in-situ sp^2 C dominant N-doped carbon, Chem. Eng. J. 381 (2020), 122510.
[29] J. Chen, C. Fang, W. Xia, T. Huang, C.H. Huang, Selective transformation of beta-lactam antibiotics by peroxymonosulfate: reaction kinetics and nonradical mechanism, Environ. Sci. Technol. 52 (2018) 1461–1470.
[30] S. Jabeen, T.J. Dines, S.A. Leharne, B.Z. Chowdhry, Raman and IR spectroscopic studies of fenamates–conformational differences in polymorphs of flufenamic acid, mefenamic acid and tolfenamic acid, Spectrochim. Acta A Mol. Biomol. Spectrosc. 96 (2012) 972–985.
[31] M. Zhou, F. Pu, Z. Wang, S. Guan, Nitrogen-doped porous carbons through KOH activation with superior performance in supercapacitors, Carbon 68 (2014) 185–194.
[32] P. Liang, C. Zhang, X. Duan, H. Sun, S. Liu, M.O. Tade, S. Wang, N-doped graphene from metal–organic frameworks for catalytic oxidation of p-hydroxylbenzoic acid: N-functionality and mechanism, ACS Sustain. Chem. Eng. 5 (2017) 2693–2701.
[33] R.P. Rocha, J. Restivo, J.P.S. Sousa, J.J.M. Órfão, M.F.R. Pereira, J.L. Figueiredo, Nitrogen-doped carbon xerogels as catalysts for advanced oxidation processes, Catal. Today 241 (2015) 73–79.
[34] Y. Fan, Y. Zhou, Y. Feng, P. Wang, X. Li, K. Shih, Fabrication of reactive flat-sheet ceramic membranes for oxidative degradation of ofloxacin by peroxymonosulfate, J. Membr. Sci. 611 (2020), 118302.
[35] X. Duan, H. Sun, Y. Wang, J. Kang, S. Wang, N-doping-induced nonradical reaction on single-walled carbon nanotubes for catalytic phenol oxidation, ACS Catal. 5 (2014) 553–559.
[36] Y. Chen, G. Zhang, H. Liu, J. Qu, Confining free radicals in close vicinity to contaminants enables ultrafast Fenton-like processes in the interspacing of MoS_2 membranes, Angew. Chem. Int. Ed. Engl. 58 (2019) 8134–8138.
[37] Y. Wang, L. Chen, C. Chen, J. Xi, H. Cao, X. Duan, Y. Xie, W. Song, S. Wang, Occurrence of both hydroxyl radical and surface oxidation pathways in N-doped layered nanocarbons for aqueous catalytic ozonation, Appl. Catal. B Environ. 254 (2019) 283–291.
[38] E.T. Yun, J.H. Lee, J. Kim, H.D. Park, J. Lee, Identifying the nonradical mechanism in the peroxymonosulfate activation process: singlet oxygenation versus mediated electron transfer, Environ. Sci. Technol. 52 (2018) 7032–7042.
[39] L. Wang, J. Jiang, S.-Y. Pang, Y. Zhou, J. Li, S. Sun, Y. Gao, C. Jiang, Oxidation of bisphenol A by nonradical activation of peroxymonosulfate in the presence of amorphous manganese dioxide, Chem. Eng. J. 352 (2018) 1004–1013.
[40] G. Fang, C. Liu, J. Gao, D.D. Dionysiou, D. Zhou, Manipulation of persistent free radicals in biochar to activate persulfate for contaminant degradation, Environ. Sci. Technol. 49 (2015) 5645–5653.
[41] G. Fang, J. Gao, C. Liu, D.D. Dionysiou, Y. Wang, D. Zhou, Key role of persistent free radicals in hydrogen peroxide activation by biochar: implications to organic contaminant degradation, Environ. Sci. Technol. 48 (2014) 1902–1910.
[42] T. Zhang, H. Zhu, J.P. Croue, Production of sulfate radical from peroxymonosulfate induced by a magnetically separable $CuFe_2O_4$ spinel in water: efficiency, stability, and mechanism, Environ. Sci. Technol. 47 (2013) 2784–2791.